

---

# Efficient Fine-Tuning of Quantized Models via Adaptive Rank and Bitwidth

---

**Changhai Zhou**

Fudan University

zhouch23@m.fudan.edu.cn

**Yuhua Zhou**

Zhejiang University

zhouyuhua@zju.edu.cn

**Qian Qiao**

Soochow University

joeqian@aliyun.com weizhongzhang@fudan.edu.cn jc@fudan.edu.cn

## Abstract

QLoRA effectively combines low-bit quantization and LoRA to achieve memory-friendly fine-tuning for large language models (LLM). Recently, methods based on SVD for continuous update iterations to initialize LoRA matrices to accommodate quantization errors have generally failed to consistently improve performance. Dynamic mixed precision is a natural idea for continuously improving the fine-tuning performance of quantized models, but previous methods often optimize low-rank subspaces or quantization components separately, without considering their synergy. To address this, we propose **QR-Adaptor**, a unified, gradient-free strategy that uses partial calibration data to jointly search the quantization components and the rank of low-rank spaces for each layer, thereby continuously improving model performance. QR-Adaptor does not minimize quantization error but treats precision and rank allocation as a discrete optimization problem guided by actual downstream performance and memory usage. Compared to state-of-the-art (SOTA) quantized LoRA fine-tuning methods, our approach achieves a 4.89% accuracy improvement on GSM8K, and in some cases even outperforms the 16-bit fine-tuned model while maintaining the memory footprint of the 4-bit setting.

## 1 Introduction

Large Language Models (LLMs) have achieved remarkable success in both language understanding and generation [Makridakis et al., 2023, Raiaan et al., 2024, Chang et al., 2024], yet adapting these powerful models to specific downstream tasks is often hindered by immense computational and memory costs [Wan et al., 2023]. Parameter-Efficient Fine-Tuning (PEFT) methods, such as Low-Rank Adaptation (LoRA) [Hu et al., 2022], address these bottlenecks by introducing lightweight low-rank updates to the core model parameters, thereby reducing the storage and compute needed for full gradient-based optimization. In parallel, quantization techniques [Gong et al., 2014, Gupta et al., 2015] compress weight matrices to fewer bits, enabling faster inference and lower memory footprints. Building on these two lines of research, QLoRA [Dettmers et al., 2023] has become a widely adopted paradigm for memory-efficient LLM fine-tuning, effectively pairing quantization with LoRA.

Recent works aim to further reduce quantization errors by adjusting the quantized weights before fine-tuning. For instance, LoftQ [Li et al., 2023] fits a portion of the error  $\mathbf{W} - \mathbf{Q}$  through SVD-based initialization, and LQ-LoRA [Guo et al., 2024] attempts a similar correction strategy. While these approaches can boost performance after *one* iteration, multiple iterative corrections sometimes degrade accuracy—as illustrated in Figure 1, where LoftQ performance declines over several rounds. This drop arises in part from a mismatch between the discrete nature of quantization and continuous

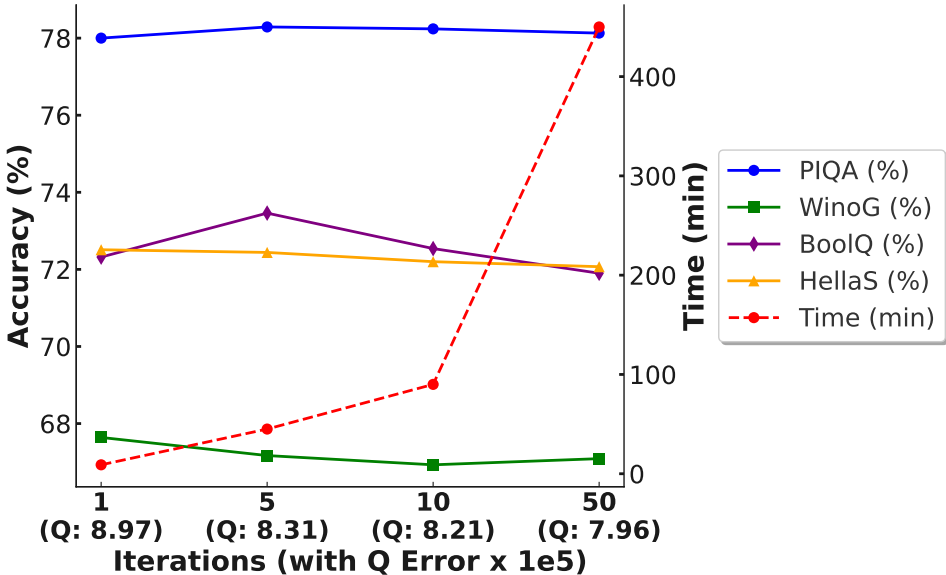


Figure 1: LoftQ iterations, quantization error, fine-tuning performance, and time cost. As the iteration count increases, the overall quantization error slightly decreases but does not yield proportional boosts in downstream performance. Moreover, the fraction of the error that can still be reduced shrinks with each iteration, ultimately fitting around 20% of the quantization error.

SVD updates, which risk shifting the model away from both  $\mathbf{Q}$  and  $\mathbf{W}$ . Additionally, methods that dynamically adjust LoRA’s rank at run time, such as AdaLoRA [Zhang et al., 2023b], may introduce extra complexity for quantized models whose robustness has already been weakened [Gong et al., 2024].

We introduce **QR-Adaptor**, an approach that aims to circumvent these shortcomings by exploring each layer’s bitwidth and LoRA level in a uniform search space. Rather than optimizing quantization and LoRA parameters in isolation—or iteratively refining continuous residuals—QR-Adaptor jointly determines each layer’s precision level ( $q_l$ ) and adaptation capacity ( $r_l$ ). This approach exploits the interplay between numerical precision and low-rank expressiveness: certain layers may demand a higher bit-width to preserve critical features, while others benefit more from an increased LoRA rank to capture complex task-specific cues. By considering both factors together, QR-Adaptor achieves more robust control over memory usage and downstream accuracy. Specifically, our method conducts a *gradient-free*, multi-objective search over discrete  $(q_l, r_l)$  pairs for each layer. To keep the computational burden comparable to a single SVD iteration, we evaluate candidate configurations only on a small *partial calibration* subset of the training data. Through this design, QR-Adaptor avoids the shortcomings of iterative SVD-based error fitting, and leverages a cohesive search strategy that systematically aligns quantization precision with LoRA’s representational power in quantized LLM fine-tuning.

To robustly explore the high-dimensional configuration space, we adopt two established multi-objective optimization methods. First, we perform a **global exploration** using a Pareto-Ranking Genetic Algorithm reminiscent of NSGA-II Deb et al. [2002], which maintains a diverse population of candidate solutions. Second, we apply **local refinement** with Bayesian optimization based on Gaussian processes, homing in on locally optimal trade-offs between performance and memory. By carefully integrating these techniques, QR-Adaptor systematically avoids the shortcomings of iterative error-fitting, improving upon baseline approaches in both efficacy and versatility. We summarize our main contributions as follows:

- We uncover the reasons why existing iterative methods, which focus on reducing quantization errors through continuous optimization, fail to consistently enhance the performance of quantized models. In particular, we find that merely refining SVD-based corrections or individually adjusting bit-widths or LoRA ranks cannot adequately boost the capabilities of quantized LLMs.

- We propose a multi-objective, gradient-free optimization strategy, QR-Adaptor, which jointly searches for the per-layer bit-width and LoRA rank. This approach integrates task-informed initialization, a Pareto-ranking genetic algorithm, and Bayesian optimization, and keeps the overhead comparable to a single SVD iteration by using calibration data.
- Our method consistently outperforms previous baselines on multiple benchmarks (e.g., achieving a 4.89% improvement in accuracy on GSM8K). In some cases, it even surpasses 16-bit fine-tuned models while requiring memory comparable to that of a 4-bit setting.

## 2 Background

In this section, we analyze why iterative methods that aim to reduce quantization errors via continuous SVD-based updates can be suboptimal when weights are constrained to a discrete lattice. We also provide optimization paths for three different fine-tuned initialization strategies in Appendix 7, illustrating that iterative fitting of quantization errors may not be able to approximate the original accuracy model, thus motivating our proposed approach.

### 2.1 Discrete Nature of Quantization

**Definition 2.1** (Quantization Operator). For a weight matrix  $\mathbf{W} \in \mathbb{R}^{d \times k}$  and quantization step  $\Delta$ , the quantization operator is defined as:

$$\text{Quantize}(\mathbf{W}) = \Delta \cdot \left\lfloor \frac{\mathbf{W}}{\Delta} + \frac{1}{2} \right\rfloor, \quad (1)$$

where  $\lfloor \cdot \rfloor$  denotes element-wise rounding. This operation projects  $\mathbf{W}$  onto the discrete lattice:

$$\mathcal{L} = \Delta \cdot \mathbb{Z}^{d \times k} \subset \mathbb{R}^{d \times k}. \quad (2)$$

**Interpretation.** This formalizes that each parameter in  $\mathbf{W}$  can only take values from a discrete set (the “lattice”) after quantization. Even small changes in real-valued space may map to the *same* discrete point under rounding, causing discontinuities in any gradient-based updates.

### 2.2 Mismatch in Continuous Approximations

Existing methods often minimize

$$\min_{\mathbf{A}, \mathbf{B}} \left\| \mathbf{W} - \underbrace{\text{Quantize}(\mathbf{W})}_{\in \mathcal{L}} - \mathbf{AB} \right\|_F. \quad (3)$$

However, this objective presumes a continuous measure of error (the Frobenius norm) even though the feasible set  $\text{Quantize}(\mathbf{W})$  is discrete.

#### Key Issues.

- *Space Duality:* The solution space for  $\mathbf{AB}$  is continuous ( $\mathbb{R}^{d \times r} \times \mathbb{R}^{r \times k}$ ), whereas  $\text{Quantize}(\mathbf{W})$  must remain in the discrete lattice  $\mathcal{L}$ . Thus,  $\text{Quantize}(\mathbf{W}) + \mathbf{AB}$  might lie outside  $\mathcal{L}$  after updates, negating any continuous gains.
- *Gradient Discontinuity:* Let  $\mathcal{P}_{\mathcal{L}}$  project onto  $\mathcal{L}$ . True gradient flow would require differentiating through  $\mathcal{P}_{\mathcal{L}}(\text{Quantize}(\mathbf{W}) + \mathbf{AB})$ . But  $\mathcal{P}_{\mathcal{L}}$  has zero gradient *almost everywhere*, making standard backpropagation ineffective for adjusting  $\mathbf{AB}$  in a discrete context.

**Implication.** Because  $\mathbf{Q} = \text{Quantize}(\mathbf{W})$  is fixed to a discrete set, continuously optimizing  $\mathbf{A}, \mathbf{B}$  to reduce  $\|\mathbf{W} - \mathbf{Q} - \mathbf{AB}\|_F$  can yield diminishing or no improvements in final performance. Each step might look beneficial in a continuous sense but fails to move to a truly better discrete state.

### 2.3 Formal Proof of Suboptimality

**Proposition 2.2.** *Let*

$$\mathbf{AB}^* = \arg \min_{\mathbf{A}, \mathbf{B}} \left\| \mathbf{W} - \text{Quantize}(\mathbf{W}) - \mathbf{AB} \right\|_F. \quad (4)$$

Then there exists a  $\mathbf{Q}' \in \mathcal{L}$  such that

$$\|\mathbf{W} - \mathbf{Q}'\|_F < \|\mathbf{W} - \text{Quantize}(\mathbf{W}) - \mathbf{AB}^*\|_F. \quad (5)$$

*Proof.* By the projection theorem:

$$\|\mathbf{W} - \mathcal{P}_{\mathcal{L}}(\mathbf{W})\|_F \leq \|\mathbf{W} - \mathbf{X}\|_F \quad \forall \mathbf{X} \in \mathcal{L}, \quad (6)$$

$$\|\mathbf{W} - \mathbf{Q}'\|_F \leq \|\mathbf{W} - \text{Quantize}(\mathbf{W}) - \mathbf{AB}^*\|_F, \quad (7)$$

where  $\mathbf{Q}' = \mathcal{P}_{\mathcal{L}}(\mathbf{W})$ . Equality holds only if  $\text{Quantize}(\mathbf{W}) + \mathbf{AB}^* \in \mathcal{L}$ , requiring  $\mathbf{AB}^*$  to exactly compensate discrete rounding errors—an event with measure zero in high dimensions.  $\square$

**Interpretation.** This proposition states that even the best continuous low-rank correction  $\mathbf{AB}^*$  *cannot* fully offset the errors introduced by discrete quantization. A strictly better discrete point  $\mathbf{Q}'$  often exists in lattice space, demonstrating that methods trying to fix  $\text{Quantize}(\mathbf{W})$  plus a real-valued  $\mathbf{AB}$  can remain suboptimal. In simpler terms, *no matter how well we approximate  $\mathbf{W} - \text{Quantize}(\mathbf{W})$  by a continuous matrix, there may be a better purely discrete solution.*

## 2.4 Manifold Analysis

We can decompose the parameter space as

$$\mathcal{M} = \mathcal{L} \oplus \{\mathbf{AB} \mid \text{rank}(\mathbf{AB}) \leq r\}. \quad (8)$$

Because  $\mathcal{L}$  is discrete and  $\{\mathbf{AB}\}$  is continuous, their sum  $\mathcal{M}$  is a hybrid space.

### Critical Observations.

- The intersection  $\mathcal{L} \cap (\text{Quantize}(\mathbf{W}) + \{\mathbf{AB}\})$  forms isolated points, underscoring the *rare alignment* needed for continuous  $\mathbf{AB}$  to fix discrete rounding completely.
- The effective search space  $\mathcal{M}_{\text{eff}} = \{\mathcal{P}_{\mathcal{L}}(\text{Quantize}(\mathbf{W}) + \mathbf{AB})\}$  has a fractal-like structure, reflecting the discontinuous jumps among discrete levels.

**Implication.** As dimension  $d \times k$  grows, the measure of  $\mathbf{AB}$  that perfectly lands in the same discrete cell as  $\mathbf{W}$  becomes negligible. This reinforces the statement that *purely continuous approximations rarely coincide with actual quantized solutions*, making Frobenius-based SVD updates unreliable for improving final performance.

## 2.5 Dynamical System Perspective

Training dynamics can be modeled by

$$\frac{d}{dt} \begin{pmatrix} \mathbf{A} \\ \mathbf{B} \end{pmatrix} = -\eta \nabla_{\mathbf{A}, \mathbf{B}} \mathcal{L} \left( \mathcal{P}_{\mathcal{L}}(\text{Quantize}(\mathbf{W}) + \mathbf{AB}) \right). \quad (9)$$

### Key Properties.

- The right-hand side is piecewise constant, with jumps on the boundaries of  $\mathcal{L}$ . Small changes in  $\mathbf{A}, \mathbf{B}$  that do not cross a boundary in  $\mathcal{L}$  produce no difference in the discrete projection.
- Eigenvalues of the Jacobian vanish when projected onto the interior of a lattice cell. This means typical continuous gradient-based methods cannot easily escape suboptimal cells since they see "flat" gradients within each cell.

**Meaning for Practical Fine-Tuning.** This piecewise constant nature implies that *iterative SVD or gradient-based fitting* will exhibit plateau-like behavior in large regions, only changing when crossing quantization boundaries. Consequently, even if  $\|\mathbf{W} - (\mathbf{Q} + \mathbf{AB})\|_F$  looks partially improved in a real-valued sense, the *actual* quantized weights remain stuck. Hence, iterative error-fitting procedures may end up stagnating.

Collectively, these findings explain why repeated SVD-based steps may reduce the *continuous* norm  $\|\mathbf{W} - \mathbf{Q}\|_F$ , yet fail to yield stable accuracy improvements under quantization. In contrast, our

approach (§3) avoids this pitfall by adopting a *gradient-free, multi-objective* strategy. Instead of directly minimizing Frobenius error in a continuous space, we evaluate each candidate (bit-width, LoRA rank) *within* the discrete quantized domain to optimize real downstream performance and memory usage.

### 3 Methodology

#### 3.1 Problem Formulation

We consider a pre-trained LLM of  $L$  layers. Each layer  $l$  has a base weight matrix  $\mathbf{W}_l \in \mathbb{R}^{d \times k}$ , which we wish to *both* quantize to a lower bit-width  $q_l$  *and* augment with a low-rank LoRA adaptation of rank  $r_l$ . Specifically, let

$$q_l \in \mathcal{Q} \quad \text{and} \quad r_l \in \mathcal{R},$$

where  $\mathcal{Q}$  is the set of all feasible bit-width values (e.g., 4, 8 bits) and  $\mathcal{R}$  the set of all feasible LoRA ranks. We unify these layer-wise assignments into a single *configuration*:

$$C = \{(q_1, r_1), (q_2, r_2), \dots, (q_L, r_L)\},$$

and let  $\mathcal{C}$  be the space of all such configurations.

**Layer-wise Quantization & LoRA.** For layer  $l$ , we apply a *quantization function* to obtain:

$$\hat{\mathbf{W}}_l^{q_l} = \text{Quantize}(\mathbf{W}_l, q_l). \quad (10)$$

We then add a *low-rank* term  $\Delta \mathbf{W}_l^{r_l} = \mathbf{A}_l \mathbf{B}_l$ , where  $\mathbf{A}_l \in \mathbb{R}^{d \times r_l}$  and  $\mathbf{B}_l \in \mathbb{R}^{r_l \times k}$ . The layer's forward pass for an input  $\mathbf{x} \in \mathbb{R}^k$  is:

$$\mathbf{y} = \hat{\mathbf{W}}_l^{q_l} \mathbf{x} + \Delta \mathbf{W}_l^{r_l} \mathbf{x}. \quad (11)$$

Hence, each layer's parameters become a combination of discrete weights  $\hat{\mathbf{W}}_l^{q_l}$  (bit-width  $q_l$ ) and a continuous LoRA update of rank  $r_l$ .

**Objective: Performance vs. Memory.** Our goal is to find a configuration  $C \in \mathcal{C}$  that yields high accuracy on a training set  $\mathcal{D}_{\text{train}}$  (evaluated on downstream tasks  $\mathcal{D}_{\text{test}}$ ) while minimizing memory usage. Let  $P(C)$  be the model's performance under configuration  $C$ , and let  $M(C)$  be its total memory footprint (including quantized weights and LoRA parameters). We combine these criteria in a single weighted objective:

$$\begin{aligned} \max_{C \in \mathcal{C}} \quad & \alpha \frac{P(C) - \mu_P}{\sigma_P} - (1 - \alpha) \frac{M(C) - \mu_M}{\sigma_M}, \\ \text{subject to} \quad & q_l \in \mathcal{Q}, r_l \in \mathcal{R}, \text{ for each } l = 1, \dots, L. \end{aligned} \quad (12)$$

Here,  $(\mu_P, \sigma_P)$  and  $(\mu_M, \sigma_M)$  are the mean and standard deviation of performance and memory, computed over sample configurations to normalize their scales. The parameter  $\alpha \in [0, 1]$  governs the trade-off: a larger  $\alpha$  places more emphasis on performance  $P(C)$ , whereas a smaller  $\alpha$  prioritizes memory reduction  $M(C)$ .

#### 3.2 QR-Adaptor Framework

Our approach differs from previous methods relying on fixed or hierarchical dynamic single configurations. We jointly explore the configuration space of quantization bits and LoRA ranks, creating a comprehensive search space that encompasses all potential optimal configurations. The main challenges in implementing this gradient-free optimization process are (a) The high-dimensional, discrete nature of the configuration space. (b) The computational cost of evaluating performance. To address these challenges, we propose QR-Adaptor, a method that effectively finds the relative optimal solution in three stages.

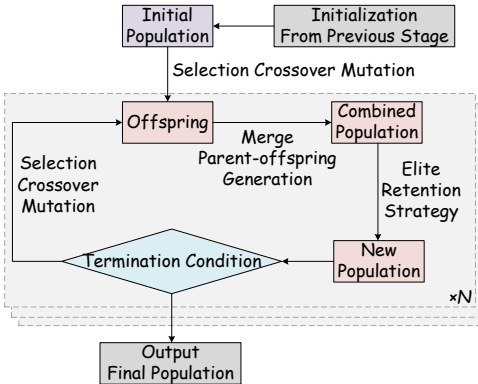


Figure 2: Detailed PRGA flow chart. The input is a set of solutions from the initialization, and the output is a set of Pareto front solutions containing multiple solutions.

**Task Information Based Initialization** Our optimization pipeline starts by estimating the *relative importance* of each layer to the downstream task. Rather than relying on gradient norms (which may fail to capture a layer’s true influence on inference), we adopt an *information-entropy* criterion:

$$I(l) = H(Y) - H(Y \mid X_l), \quad (13)$$

where  $H(Y)$  is the entropy of the model's outputs, and  $H(Y | X_l)$  is the conditional entropy given the  $l$ -th layer's intermediate representation. Layers with a higher  $I(l)$  exert greater impact on final predictions. Empirically, we find (Appendix 13.1) that this entropy-based approach outperforms gradient-norm heuristics in selecting effective layers for bit-width and rank adjustments.

Concretely, we initialize per-layer quantization bits  $\{q_l\}$  by assigning larger  $q_l$  to layers with higher importance scores and smaller  $q_l$  to those deemed less critical. After quantizing the model with these initial bits, we recompute layer importance under quantization and then allocate LoRA ranks  $\{r_l\}$ : layers that remain most vital post-quantization receive larger  $r_l$ , while others get reduced ranks. This two-step procedure narrows the search space to promising configurations from the outset, guiding subsequent multi-objective optimization toward higher accuracy and lower memory usage.

**Global Exploration with PRGA** In LLM fine-tuning, quantization bit and LoRA rank can be conceptualized as genes, with the resulting performance and memory usage analogous to phenotypic expressions in a population. Inspired by NSGA-II’s Deb et al. [2002] proven success in multi-objective optimization, we adapted its mechanisms to develop PRGA (Pareto Ranking Genetic Algorithm). PRGA explores the combined solution space of bits and ranks to identify the optimal Pareto frontier, simultaneously balancing performance and memory usage in LLM fine-tuning. This efficient multi-objective optimization algorithm uses an elitist selection approach to evolve a population of configurations, each represented as  $C = \{(q_l, r_l)\}_{l=1}^L$ , where  $q_l$  and  $r_l$  denote the quantization bits and LoRA rank for layer  $l$ , respectively. PRGA iteratively applies selection, crossover, and mutation operations to the population, aiming to simultaneously maximize performance and minimize memory usage. The algorithm progresses until it reaches a predefined stopping criterion or a maximum number of iterations, whichever comes first. Once finished, the algorithm ultimately produces a Pareto frontier that represents the optimal trade-offs between our competing objectives.

Before introducing the PRGA flow, we first introduce some key foundational concepts. In a multi-objective minimization problem with  $n$  objective components  $f_i(x)$ ,  $i = 1, \dots, n$ , the Pareto Dominance Relationship is defined between any two decision variables  $X_a$  and  $X_b$ . We say that  $X_a$  dominates  $X_b$  if for all  $i \in \{1, 2, \dots, n\}$ ,  $f_i(X_a) \leq f_i(X_b)$ , and there exists at least one  $i \in \{1, 2, \dots, n\}$  such that  $f_i(X_a) < f_i(X_b)$ . A Non-dominated Solution is a decision variable that is not dominated by any other decision variable in the set. The concept of Pareto Rank is used to categorize solutions within a set. Non-dominated solutions are assigned a Pareto rank of 1. After removing these rank 1 solutions from the set, the remaining non-dominated solutions are assigned a Pareto rank of 2. This process continues iteratively, assigning increasing ranks to subsequent layers of non-dominated solutions until all solutions in the set have been ranked.

As illustrated in Algorithm 1, we employ the Pareto Ranking to sort all individuals within the population. To address solutions with identical Pareto ranks, we use the crowding distance  $d$  for

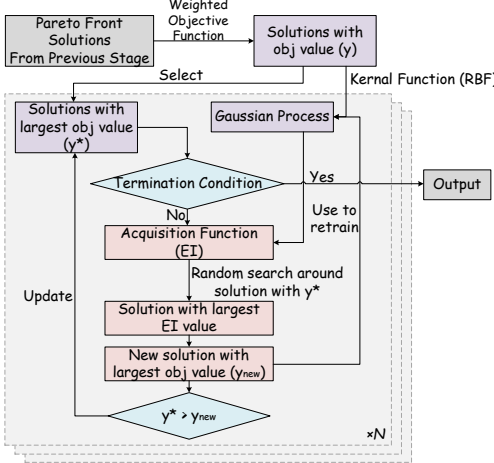


Figure 3: Detailed Bayesian optimization flow chart. The input is the Pareto front solution set from the global search, and the output is a set of optimal solutions obtained according to the requirements.

further differentiation within each Pareto rank. The detailed calculation of the crowding distance is presented in Algorithm 2.

Elite retention, a method simulating natural elimination, is performed after calculating the Pareto rank and crowding distance of all individuals in a generation. This process begins by combining the parent and offspring populations into a merged population. To generate the next generation, we start with the lowest Pareto rank and transfer entire layers of individuals from the merged population to the new population, moving progressively to higher ranks. This continues until we reach a layer that cannot be fully accommodated in the new population. For this partially accommodated layer, we sort its individuals based on their crowding distance in descending order and add them sequentially to the new population until it reaches its full capacity.

For the crossover and mutation operations, we employ methods analogous to Simulated Binary Crossover (SBX) and Polynomial Mutation, respectively. These methods are adapted to operate on  $L$  pairs of positive integers  $(q_l, r_l)$ . The detailed procedures for these operations are presented in Algorithm 3 for the crossover and Algorithm 4 for the mutation. By applying these adapted SBX and polynomial mutation operations, we can effectively evolve the population of solutions represented by integer pairs, balancing exploration and exploitation.

The PRGA process, shown in Figure 2, begins by generating an initial population of size  $N$  through controlled random variations based on the previous stage’s configuration. It then creates offspring using selection, crossover, and mutation operations. The parent and offspring populations are combined and subsequently fastly fine-tuned and validated on a subset of the training dataset. The resulting performance and memory metrics are used to calculate Pareto ranks for each individual. Next, the algorithm applies an elite retention strategy combined with crowding distance calculation to select individuals for the new population. This cycle repeats, generating consecutive generations until the termination condition is met, effectively exploring the solution space to optimize both performance and memory usage simultaneously.

**Local Refinement with Bayesian Optimization** While PRGA effectively explores the global configuration space, it may not precisely capture local optima near the Pareto front. To further refine these solutions, we employ Bayesian optimization, a technique renowned for its ability to optimize expensive black-box functions with uncertainty quantification. We initiate this process by utilizing the solutions from the PRGA-generated Pareto front as our initial sampling points. For each point, we use these configurations to quickly fine-tune the model and test to obtain actual performance and memory usage. We then compute its corresponding weighted objective function value  $y$  using the predefined objective function (Equation 12) and specified weight preferences. These  $y$  values serve a dual purpose: firstly, they are combined with the covariance matrix  $K$ , which is constructed using the radial basis function (RBF) kernel to quantify similarities between sample points, to build a Gaussian process model; secondly, they enable us to identify the best-performing point, which becomes the focal point for subsequent searches.

The next phase involves employing a random search strategy to select new sampling points in the vicinity of this top-performing configuration. For each newly selected sampling point  $x^*$ , we leverage the Gaussian process to estimate its predicted value and associated uncertainty using the following equations:

$$\begin{aligned}\mu(x^*) &= m(x^*) + K(x^*, X)K(X, X)^{-1}(y - m(X)) \\ \sigma^2(x^*) &= k(x^*, x^*) - K(x^*, X)K(X, X)^{-1}K(X, x^*)\end{aligned}\tag{14}$$

where  $m(x^*)$  is the prior mean function,  $K(x^*, X)$  is the covariance between the new point and the existing points, and  $K(X, X)$  is the covariance matrix of the existing points.

We then employ the Expected Improvement (EI) as the acquisition function, calculating it using the following formula:

$$\begin{aligned}EI(x^*) &= \sigma(x^*) (Z \cdot \Phi(Z) + \phi(Z)) \\ \text{and } Z &= \frac{\mu(x^*) - y_{\text{best}}}{\sigma(x^*)}.\end{aligned}\tag{15}$$

where  $\Phi(Z)$  is the cumulative distribution function of the standard normal distribution, while  $\phi(Z)$  is its probability density function and  $y_{\text{best}}$  is the best objective value among all points.

We select the point with the largest EI value as the next evaluation point and quickly fine-tune the LLM using this configuration. We then test to obtain the performance and memory usage, which are used to calculate the objective function value, and this new point is compared with the previous best point. If it proves to be a better choice, it can be updated as the optimal point and the search for the next iteration proceeds near it; otherwise, we continue searching near the original optimal point. Regardless of whether the best point is updated, the new point and its objective function value are incorporated into the training dataset to update the Gaussian process model before beginning the next iteration. This process repeats until a predefined termination condition is met, such as reaching maximum iterations, meeting a convergence criterion, or hitting a time limit. The detailed flowchart is shown in Figure 3.

The solution set obtained through this Bayesian optimization process offers a refined representation of high-quality configurations, effectively capturing the trade-offs between performance and memory usage. This iterative refinement process culminates in a final set of configurations that represent the best balance of our objectives based on the specified preferences. By presenting these optimized configurations as the final output, our approach enables practitioners to directly choose suitable configuration that aligns with their specific performance requirements and memory constraints.

## 4 Evaluation

In this section, we first introduce the experimental setup, including datasets, models, baselines, and implementation details. All hyperparameters aside from rank value and bit-width are kept consistent with the baselines. Additional results are provided in Appendix 10 due to space constraints:

- **Extended Experimental Results:** Further results across different models are detailed in Appendix 10.1, Appendix 10.2, and Appendix 10.6 and Appendix 10.7.
- **Impact of Higher LoRA Ranks on Larger Datasets:** Evaluations of our method on larger datasets with higher LoRA ranks are detailed in Appendix 10.3.
- **Training Time Comparison:** We analyze the training time efficiency of our method in Appendix 10.4.
- **Fair Bit-width Configuration Comparison:** A fairer comparison of quantization methods with consistent bit-width configurations is given in Appendix 10.5.

We conduct ablation studies to assess the impact of different components on performance. We demonstrate the necessity of the three-stage process by removing one stage at a time. We also perform a sensitivity analysis of PRGA hyperparameters, as presented in Appendix 13.

### 4.1 Experimental Setup

**Datasets and LLMs.** We utilize the Alpaca52k and hc3 [Taori et al., 2023] for fine-tuning and evaluate the zero-shot performance of these LLMs on benchmarks including BoolQ [Clark et al.,

Table 1: Performance comparison of different methods across various bit-width configurations on Llama3.1-8B. Superscripts on LoftQ bits indicate the number of initialization iterations. Bold figures represent the best performance for a given model and task, while underlined figures indicate the second-best. Accuracy is reported as %.

	Method	Bit	ARC(C)	ARC(E)	BoolQ	GSM8K	HellaS	OBQA	PIQA	WinoG	Average
Rank = 8	LoRA	16	56.14	<u>83.88</u>	83.18	<u>54.36</u>	79.44	45.20	<u>82.10</u>	<b>75.30</b>	69.95
	QLoRA	8	<b>57.08</b>	83.46	82.48	53.75	<u>79.63</u>	<b>46.00</b>	<u>82.10</u>	74.59	69.89
	QLoRA	4	54.35	82.41	82.08	44.35	78.82	44.20	81.50	73.64	67.67
	AdaLoRA	16	52.90	81.99	81.87	50.57	78.65	45.00	81.34	73.95	68.28
	AdaLoRA	8	52.90	81.86	82.05	49.96	78.65	44.80	81.34	74.43	68.25
	AdaLoRA	4	51.28	80.98	80.61	37.83	77.36	42.80	80.74	72.53	65.51
	LoftQ	<sup>4<sup>1</sup></sup>	54.86	82.74	82.26	51.40	78.65	<b>46.00</b>	81.45	73.24	68.82
	LoftQ	<sup>4<sup>5</sup></sup>	52.65	81.82	81.53	39.65	78.50	43.40	81.39	72.69	66.45
Rank = 16	LoftQ	<sup>4<sup>10</sup></sup>	51.88	81.31	79.66	38.44	78.01	43.20	81.12	71.98	65.70
	QR-Adaptor	5.45	<u>56.83</u>	<b>84.12</b>	<u>83.38</u>	<b>56.29</b>	<u>80.93</u>	45.80	<b>82.92</b>	<u>75.10</u>	<b>70.67</b>
	LoRA	16	<u>56.74</u>	<u>83.63</u>	83.00	<u>54.13</u>	<u>79.51</u>	44.40	<u>81.83</u>	74.43	69.70
	QLoRA	8	<u>56.23</u>	82.91	82.66	53.68	79.46	<b>46.00</b>	81.66	<u>74.74</u>	69.67
	QLoRA	4	53.84	81.99	82.11	44.66	78.76	44.40	81.72	73.09	67.57
	AdaLoRA	16	53.07	82.03	81.99	50.11	78.61	45.40	81.28	74.11	68.33
	AdaLoRA	8	53.33	82.03	82.11	49.13	78.57	45.20	81.34	73.79	68.19
	AdaLoRA	4	50.85	80.72	80.73	37.98	77.34	42.80	80.52	73.16	65.51
Rank = 32	LoftQ	<sup>4<sup>1</sup></sup>	55.12	82.58	82.69	49.81	78.82	45.80	81.28	74.27	68.80
	LoftQ	<sup>4<sup>5</sup></sup>	53.92	82.32	81.56	42.00	78.54	43.80	81.56	72.77	67.06
	LoftQ	<sup>4<sup>10</sup></sup>	52.90	81.69	81.56	39.88	78.64	43.80	81.07	71.98	66.44
	QR-Adaptor	5.45	<u>56.83</u>	<b>84.12</b>	<u>83.38</u>	<b>56.29</b>	<u>80.93</u>	45.80	<b>82.92</b>	<u>75.10</u>	<b>70.67</b>

2019], PIQA [Bisk et al., 2020], HellaSwag [Zellers et al., 2019], WinoGrande [Sakaguchi et al., 2021], ARC-easy [Clark et al., 2018], ARC-challenge [Clark et al., 2018], OpenbookQA [Mihaylov et al., 2018], and MMLU Hendrycks et al. [2021]. The models used in our experiments are Llama2 Touvron et al. [2023] and Llama3.1 Grattafiori et al. [2024].

**Baselines.** We compare our method against several baselines: without tuning, LoRA Hu et al. [2022], QLoRA Dettmers et al. [2023], Adalora Zhang et al. [2023b], LoftQ Li et al. [2023], and LQ-LoRA Guo et al. [2024]. We evaluated the performance of LoftQ with different iteration numbers. For Adalora, which dynamically allocates ranks based on the average rank budget, we set the budget to 8 and 64. Finally, for LQ-LoRA, which allocates quantization bit-width based on the average weight bit-width budget and quantization error, we set the bit-width budget to 4.

**Implementation Details.** We utilize the following configurations: *PyTorch* version 2.1.2, *Bit-sandBytes* library version 0.43.1, *Transformers* library version 4.41.0, *PEFT* library version 0.11.1, *Optuna* library version 3.6.1, *CUDA* version 12.4, *GPU*: NVIDIA L20 GPU. *Operating System*: Ubuntu. Concise implementation details are provided in the Appendix 12. We define the population size as 5 and generate 1 new offspring in each iteration. The second and third phases were iterated 5 times.

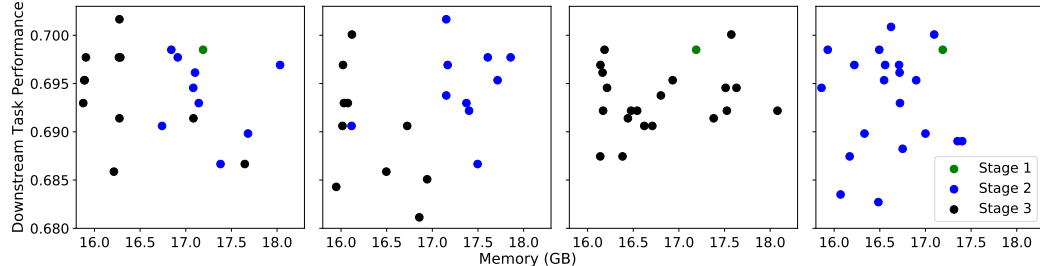


Figure 4: From left to right, the actual measured performance and memory usage of the configurations generated by QR-Adaptor, QR-Adaptor without stage1, QR-Adaptor without stage2, and QR-Adaptor without stage3 are shown. Different colors represent the configurations generated at different stages.

## 4.2 Main Results

We present the performance comparison of LLaMA3.1 on commonsense understanding tasks in Table 1. For practical deployment, we exclude the 2-bit configuration in mixed-precision setups, as it does not significantly reduce memory usage. Results with 2-bit configurations are shown in Appendix 10.7. Our method achieves or surpasses the performance of 16-bit fine-tuned models while maintaining the same memory footprint as the 4-bit models.

As mentioned, LoftQ outperforms 4-bit QLoRA after one iteration, but its performance degrades with more iterations. This is due to the mismatch between continuous error correction and discrete quantization. AdaLoRA, which dynamically adjusts LoRA rank during fine-tuning, is less effective for quantized models, as the quantization process introduces discrete constraints incompatible with dynamic rank changes. Additional results for longer training epochs are available in Appendix 10.6.

QR-Adaptor jointly optimizes bit-width and LoRA rank, balancing precision and adaptation capacity for superior performance. Our results confirm that jointly optimizing these parameters leads to better downstream performance. Furthermore, QR-Adaptor allocates resources more efficiently by assigning higher LoRA ranks to critical layers and higher precision to important layers, achieving high accuracy with low memory usage.

Due to page limitations, please see Appendix 10 for more experimental results and analysis.

## 4.3 Ablation Study

We use the WinoGrande benchmark as an example for the ablation study to evaluate the role of each stage in QR-Adapto. As shown in Figure 4, it is evident that excluding PRGA and Bayesian optimization leads to uneven exploration of the search space—one is too broad and the other too concentrated—since they represent the extrapolation and interpolation capabilities, respectively. Excluding stage 1 results in overly scattered exploration because PRGA starts from a random search without an initialization point. However, it still manages to explore the theoretically optimal region in the upper-left corner, demonstrating the strong capabilities of PRGA and Bayesian optimization. In contrast, the complete three-stage QR-Adaptor shows the advantage of first conducting a broad exploration around the initialization point, followed by interpolation near promising solutions to further optimize and identify better configuration.

## 5 Related Work

**LLM Quantization.** The field of LLM quantization has witnessed substantial progress, driven by the need for efficient model deployment. Recent research has introduced several innovative approaches. Frantar et al. [2023] have developed GPTQ, which achieves 4-bit precision with layer-wise quantization. Lin et al. [2023] have proposed AWQ, which improves accuracy for heavily quantized models. Yao et al. [2022] have introduced ZeroQuant, which preserves zero-shot capabilities at lower bit widths. Dettmers et al. [2022] have presented LLM.int8(), which enables 8-bit quantization for consumer hardware. Kim et al. [2023] have combined quantization with pruning and knowledge distillation in SqueezeLLM. Guan et al. [2024] have optimized the balance between compression and performance through mixed-precision quantization with APTQ. These developments significantly enhance the efficiency of LLMs.

**Parameter Efficient Fine-Tuning.** PEFT techniques have become crucial for enhancing LLMs without increasing inference overhead. Recent innovations have expanded the field. Dettmers et al. [2023] have introduced QLoRA, which combines 4-bit quantization with low-rank adapters. Li et al. [2023] have presented LoftQ, which alternates between quantization and low-rank approximation steps. Berman and Peherstorfer [2024] have introduced CoLoRA for accelerating the prediction of solution fields under new parameters. AdaLoRA Zhang et al. [2023a] proposes adaptive budget allocation for low-rank updates, while LQ-LoRA Guo et al. [2023] combines low-rank decomposition with quantization for efficient fine-tuning under memory constraints. Additionally, Zhou et al. [2024] have introduced RankAdaptor, which is a hierarchical dynamic low-rank adaptation method for structural pruned LLMs. These advancements offer innovative solutions for efficient LLM fine-tuning across diverse applications.

## 6 Conclusion

In this work, we propose QR-Adaptor, a unified, gradient-free method that uses partial calibration data to simultaneously optimize the precision and LoRA rank of each model layer. By focusing on the discrete nature of quantization and low-rank spaces and optimizing them within a task-driven framework, QR-Adaptor overcomes the limitations of iterative error-fitting techniques and rank-adaptive methods unsuitable for quantization. Our extensive experiments demonstrate that QR-Adaptor consistently outperforms existing baselines, achieving better performance than 16-bit fine-tuned models while maintaining a 4-bit memory footprint. These results highlight the importance of integrating quantization and low-rank matrices into a single, cohesive optimization process, driven by actual performance and memory efficiency.

## Impact Statement

This paper presents work whose goal is to advance the field of Machine Learning. There are many potential societal consequences of our work, none of which we feel must be specifically highlighted here.

## References

Jules Berman and Benjamin Peherstorfer. Colora: Continuous low-rank adaptation for reduced implicit neural modeling of parameterized partial differential equations, 2024. URL <https://arxiv.org/abs/2402.14646>.

Yonatan Bisk, Rowan Zellers, Jianfeng Gao, Yejin Choi, et al. Piqa: Reasoning about physical commonsense in natural language. In *Proceedings of the AAAI conference on artificial intelligence*, volume 34, pages 7432–7439, 2020.

Yupeng Chang, Xu Wang, Jindong Wang, Yuan Wu, Linyi Yang, Kajie Zhu, Hao Chen, Xiaoyuan Yi, Cunxiang Wang, Yidong Wang, et al. A survey on evaluation of large language models. *ACM Transactions on Intelligent Systems and Technology*, 15(3):1–45, 2024.

Christopher Clark, Kenton Lee, Ming-Wei Chang, Tom Kwiatkowski, Michael Collins, and Kristina Toutanova. Boolq: Exploring the surprising difficulty of natural yes/no questions. In *Proceedings of the 2019 Conference of the North American Chapter of the Association for Computational Linguistics: Human Language Technologies, Volume 1 (Long and Short Papers)*, pages 2924–2936, 2019.

Peter Clark, Isaac Cowhey, Oren Etzioni, Tushar Khot, Ashish Sabharwal, Carissa Schoenick, and Oyvind Tafjord. Think you have solved question answering? try arc, the ai2 reasoning challenge. *arXiv preprint arXiv:1803.05457*, 2018.

Kalyanmoy Deb, Amrit Pratap, Sameer Agarwal, and TAMT Meyarivan. A fast and elitist multiobjective genetic algorithm: Nsga-ii. *IEEE transactions on evolutionary computation*, 6(2):182–197, 2002.

Tim Dettmers, Mike Lewis, Younes Belkada, and Luke Zettlemoyer. Llm. int8 (): 8-bit matrix multiplication for transformers at scale. *CoRR*, abs/2208.07339, 2022. URL <http://arxiv.org/abs/2208.07339>.

Tim Dettmers, Artidoro Pagnoni, Ari Holtzman, and Luke Zettlemoyer. Qlora: Efficient finetuning of quantized llms. *arXiv preprint arXiv:2305.14314*, 2023.

Elias Frantar, Sahar Ashkboos, Torsten Hoefer, and Dan Alistarh. Gptq: Accurate post-training quantization for generative pre-trained transformers. In *The Eleventh International Conference on Learning Representations (ICLR)*, 2023.

Yunchao Gong, Liu Liu, Ming Yang, and Lubomir Bourdev. Compressing deep convolutional networks using vector quantization. *arXiv preprint arXiv:1412.6115*, 2014.

Zhuocheng Gong, Jiahao Liu, Jingang Wang, Xunliang Cai, Dongyan Zhao, and Rui Yan. What makes quantization for large language models hard? an empirical study from the lens of perturbation, 2024. URL <https://arxiv.org/abs/2403.06408>.

Aaron Grattafiori, Abhimanyu Dubey, Abhinav Jauhri, Abhinav Pandey, Abhishek Kadian, Ahmad Al-Dahle, Aiesha Letman, Akhil Mathur, Alan Schelten, Alex Vaughan, Amy Yang, Angela Fan, Anirudh Goyal, Anthony Hartshorn, Aobo Yang, Archi Mitra, Archie Sravankumar, Artem Korenev, Arthur Hinsvark, Arun Rao, Aston Zhang, Aurelien Rodriguez, Austen Gregerson, Ava Spataru, Baptiste Roziere, Bethany Biron, Binh Tang, Bobbie Chern, Charlotte Caucheteux, Chaya Nayak, Chloe Bi, Chris Marra, Chris McConnell, Christian Keller, Christophe Touret, Chunyang Wu, Corinne Wong, Cristian Canton Ferrer, Cyrus Nikolaidis, Damien Allonsius, Daniel Song, Danielle Pintz, Danny Livshits, Danny Wyatt, David Esiobu, Dhruv Choudhary, Dhruv Mahajan, Diego Garcia-Olano, Diego Perino, Dieuwke Hupkes, Egor Lakomkin, Ehab AlBadawy, Elina Lobanova, Emily Dinan, Eric Michael Smith, Filip Radenovic, Francisco Guzmán, Frank Zhang, Gabriel Synnaeve, Gabrielle Lee, Georgia Lewis Anderson, Govind Thattai, Graeme Nail, Gregoire Mialon, Guan Pang, Guillem Cucurell, Hailey Nguyen, Hannah Korevaar, Hu Xu, Hugo Touvron, Iliyan Zarov, Imanol Arrieta Ibarra, Isabel Kloumann, Ishan Misra, Ivan Evtimov, Jack Zhang, Jade Copet, Jaewon Lee, Jan Geffert, Jana Vranes, Jason Park, Jay Mahadeokar, Jeet Shah, Jelmer van der Linde, Jennifer Billock, Jenny Hong, Jenya Lee, Jeremy Fu, Jianfeng Chi, Jianyu Huang, Jiawen Liu, Jie Wang, Jiecao Yu, Joanna Bitton, Joe Spisak, Jongsoo Park, Joseph Rocca, Joshua Johnstun, Joshua Saxe, Junteng Jia, Kalyan Vasudevan Alwala, Karthik Prasad, Kartikeya Upasani, Kate Plawiak, Ke Li, Kenneth Heafield, Kevin Stone, Khalid El-Arini, Krithika Iyer, Kshitiz Malik, Kuenley Chiu, Kunal Bhalla, Kushal Lakhota, Lauren Rantala-Yeary, Laurens van der Maaten, Lawrence Chen, Liang Tan, Liz Jenkins, Louis Martin, Lovish Madaan, Lubo Malo, Lukas Blecher, Lukas Landzaat, Luke de Oliveira, Madeline Muzzi, Mahesh Pasupuleti, Mannat Singh, Manohar Paluri, Marcin Kardas, Maria Tsimpoukelli, Mathew Oldham, Mathieu Rita, Maya Pavlova, Melanie Kambadur, Mike Lewis, Min Si, Mitesh Kumar Singh, Mona Hassan, Naman Goyal, Narjes Torabi, Nikolay Bashlykov, Nikolay Bogoychev, Niladri Chatterji, Ning Zhang, Olivier Duchenne, Onur Çelebi, Patrick Alrassy, Pengchuan Zhang, Pengwei Li, Petar Vasic, Peter Weng, Prajjwal Bhargava, Pratik Dubal, Praveen Krishnan, Punit Singh Koura, Puxin Xu, Qing He, Qingxiao Dong, Ragavan Srinivasan, Raj Ganapathy, Ramon Calderer, Ricardo Silveira Cabral, Robert Stojnic, Roberta Raileanu, Rohan Maheswari, Rohit Girdhar, Rohit Patel, Romain Sauvestre, Ronnie Polidoro, Roshan Sumbaly, Ross Taylor, Ruan Silva, Rui Hou, Rui Wang, Saghar Hosseini, Sahana Chennabasappa, Sanjay Singh, Sean Bell, Seohyun Sonia Kim, Sergey Edunov, Shaoliang Nie, Sharan Narang, Sharath Raparth, Sheng Shen, Shengye Wan, Shruti Bhosale, Shun Zhang, Simon Vandenhende, Soumya Batra, Spencer Whitman, Sten Sootla, Stephane Collot, Suchin Gururangan, Sydney Borodinsky, Tamar Herman, Tara Fowler, Tarek Sheasha, Thomas Georgiou, Thomas Scialom, Tobias Speckbacher, Todor Mihaylov, Tong Xiao, Ujjwal Karn, Vedanuj Goswami, Vibhor Gupta, Vignesh Ramanathan, Viktor Kerkez, Vincent Gonguet, Virginie Do, Vish Vogeti, Vitor Albiero, Vladan Petrovic, Weiwei Chu, Wenhan Xiong, Wenying Fu, Whitney Meers, Xavier Martinet, Xiaodong Wang, Xiaofang Wang, Xiaoqing Ellen Tan, Xide Xia, Xinfeng Xie, Xuchao Jia, Xuewei Wang, Yaelle Goldschlag, Yashesh Gaur, Yasmine Babaei, Yi Wen, Yiwen Song, Yuchen Zhang, Yue Li, Yuning Mao, Zacharie Delpierre Coudert, Zheng Yan, Zhengxing Chen, Zoe Papakipos, Aaditya Singh, Aayushi Srivastava, Abha Jain, Adam Kelsey, Adam Shajnfeld, Adithya Gangidi, Adolfo Victoria, Ahuva Goldstand, Ajay Menon, Ajay Sharma, Alex Boesenberg, Alexei Baevski, Allie Feinstein, Amanda Kallet, Amit Sangani, Amos Teo, Anam Yunus, Andrei Lupu, Andres Alvarado, Andrew Caples, Andrew Gu, Andrew Ho, Andrew Poulton, Andrew Ryan, Ankit Ramchandani, Annie Dong, Annie Franco, Anuj Goyal, Aparajita Saraf, Arkabandhu Chowdhury, Ashley Gabriel, Ashwin Bharambe, Assaf Eisenman, Azadeh Yazdan, Beau James, Ben Maurer, Benjamin Leonhardi, Bernie Huang, Beth Loyd, Beto De Paola, Bhargavi Paranjape, Bing Liu, Bo Wu, Boyu Ni, Braden Hancock, Bram Wasti, Brandon Spence, Brani Stojkovic, Brian Gamido, Britt Montalvo, Carl Parker, Carly Burton, Catalina Mejia, Ce Liu, Changhan Wang, Changkyu Kim, Chao Zhou, Chester Hu, Ching-Hsiang Chu, Chris Cai, Chris Tindal, Christoph Feichtenhofer, Cynthia Gao, Damon Civin, Dana Beaty, Daniel Kreymer, Daniel Li, David Adkins, David Xu, Davide Testuggine, Delia David, Devi Parikh, Diana Liskovich, Didem Foss, Dingkang Wang, Duc Le, Dustin Holland, Edward Dowling, Eissa Jamil, Elaine Montgomery, Eleonora Presani, Emily Hahn, Emily Wood, Eric-Tuan Le, Erik Brinkman, Esteban Arcaute, Evan Dunbar, Evan Smothers, Fei Sun, Felix Kreuk, Feng Tian, Filippos Kokkinos, Firat Ozgenel, Francesco Caggioni, Frank Kanayet, Frank Seide, Gabriela Medina Florez, Gabriella Schwarz, Gada Badeer, Georgia Swee,

Gil Halpern, Grant Herman, Grigory Sizov, Guangyi, Zhang, Guna Lakshminarayanan, Hakan Inan, Hamid Shojanazeri, Han Zou, Hannah Wang, Hanwen Zha, Haroun Habeeb, Harrison Rudolph, Helen Suk, Henry Aspegen, Hunter Goldman, Hongyuan Zhan, Ibrahim Damlaj, Igor Molybog, Igor Tufanov, Ilias Leontiadis, Irina-Elena Veliche, Itai Gat, Jake Weissman, James Geboski, James Kohli, Janice Lam, Japhet Asher, Jean-Baptiste Gaya, Jeff Marcus, Jeff Tang, Jennifer Chan, Jenny Zhen, Jeremy Reizenstein, Jeremy Teboul, Jessica Zhong, Jian Jin, Jingyi Yang, Joe Cummings, Jon Carvill, Jon Shepard, Jonathan McPhie, Jonathan Torres, Josh Ginsburg, Junjie Wang, Kai Wu, Kam Hou U, Karan Saxena, Kartikay Khandelwal, Katayoun Zand, Kathy Matosich, Kaushik Veeraghavan, Kelly Michelena, Keqian Li, Kiran Jagadeesh, Kun Huang, Kunal Chawla, Kyle Huang, Lailin Chen, Lakshya Garg, Lavender A, Leandro Silva, Lee Bell, Lei Zhang, Liangpeng Guo, Licheng Yu, Liron Moshkovich, Luca Wehrstedt, Madien Khabsa, Manav Avalani, Manish Bhatt, Martynas Mankus, Matan Hasson, Matthew Lennie, Matthias Reso, Maxim Groshev, Maxim Naumov, Maya Lathi, Meghan Keneally, Miao Liu, Michael L. Seltzer, Michal Valko, Michelle Restrepo, Mihir Patel, Mik Vyatskov, Mikayel Samvelyan, Mike Clark, Mike Macey, Mike Wang, Miquel Jubert Hermoso, Mo Metanat, Mohammad Rastegari, Munish Bansal, Nandhini Santhanam, Natascha Parks, Natasha White, Navyata Bawa, Nayan Singhal, Nick Egebo, Nicolas Usunier, Nikhil Mehta, Nikolay Pavlovich Laptev, Ning Dong, Norman Cheng, Oleg Chernoguz, Olivia Hart, Omkar Salpekar, Ozlem Kalinli, Parkin Kent, Parth Parekh, Paul Saab, Pavan Balaji, Pedro Rittner, Philip Bontrager, Pierre Roux, Piotr Dollar, Polina Zvyagina, Prashant Ratanchandani, Pritish Yuvraj, Qian Liang, Rachad Alao, Rachel Rodriguez, Rafi Ayub, Raghotham Murthy, Raghu Nayani, Rahul Mitra, Rangaprabhu Parthasarathy, Raymond Li, Rebekkah Hogan, Robin Battey, Rocky Wang, Russ Howes, Ruty Rinott, Sachin Mehta, Sachin Siby, Sai Jayesh Bondu, Samyak Datta, Sara Chugh, Sara Hunt, Sargun Dhillon, Sasha Sidorov, Satadru Pan, Saurabh Mahajan, Saurabh Verma, Seiji Yamamoto, Sharadh Ramaswamy, Shaun Lindsay, Shaun Lindsay, Sheng Feng, Shenghao Lin, Shengxin Cindy Zha, Shishir Patil, Shiva Shankar, Shuqiang Zhang, Shuqiang Zhang, Sinong Wang, Sneha Agarwal, Soji Sajuyigbe, Soumith Chintala, Stephanie Max, Stephen Chen, Steve Kehoe, Steve Satterfield, Sudarshan Govindaprasad, Sumit Gupta, Summer Deng, Sungmin Cho, Sunny Virk, Suraj Subramanian, Sy Choudhury, Sydney Goldman, Tal Remez, Tamar Glaser, Tamara Best, Thilo Koehler, Thomas Robinson, Tianhe Li, Tianjun Zhang, Tim Matthews, Timothy Chou, Tzook Shaked, Varun Vontimitta, Victoria Ajayi, Victoria Montanez, Vijai Mohan, Vinay Satish Kumar, Vishal Mangla, Vlad Ionescu, Vlad Poenaru, Vlad Tiberiu Mihailescu, Vladimir Ivanov, Wei Li, Wenchen Wang, Wenwen Jiang, Wes Bouaziz, Will Constable, Xiaocheng Tang, Xiaoqian Wu, Xiaolan Wang, Xilun Wu, Xinbo Gao, Yaniv Kleinman, Yanjun Chen, Ye Hu, Ye Jia, Ye Qi, Yenda Li, Yilin Zhang, Ying Zhang, Yossi Adi, Youngjin Nam, Yu, Wang, Yu Zhao, Yuchen Hao, Yundi Qian, Yunlu Li, Yuzi He, Zach Rait, Zachary DeVito, Zef Rosnbrick, Zhaoduo Wen, Zhenyu Yang, Zhiwei Zhao, and Zhiyu Ma. The llama 3 herd of models, 2024. URL <https://arxiv.org/abs/2407.21783>.

Zhaoyi Guan, Hongyi Huang, Yihan Su, Haoxiang Huang, Ngai Wong, and Huazhong Yu. Aptq: Attention-aware post-training mixed-precision quantization for large language models. *arXiv preprint arXiv:2402.14866*, 2024.

Han Guo, Philip Greengard, Eric Xing, and Yoon Kim. Lq-lora: Low-rank plus quantized matrix decomposition for efficient language model finetuning. *ICLR* 2024, 2023.

Han Guo, Philip Greengard, Eric Xing, and Yoon Kim. LQ-loRA: Low-rank plus quantized matrix decomposition for efficient language model finetuning. In *The Twelfth International Conference on Learning Representations*, 2024. URL <https://openreview.net/forum?id=xw29VvOMmU>.

Suyog Gupta, Ankur Agrawal, Kailash Gopalakrishnan, and Pritish Narayanan. Deep learning with limited numerical precision. In *International conference on machine learning*, pages 1737–1746. PMLR, 2015.

Dan Hendrycks, Collin Burns, Steven Basart, Andy Zou, Mantas Mazeika, Dawn Song, and Jacob Steinhardt. Measuring massive multitask language understanding. In *International Conference on Learning Representations*, 2021. URL <https://openreview.net/forum?id=d7KBjmI3GmQ>.

Edward J. Hu, Yelong Shen, Phillip Wallis, Zeyuan Allen-Zhu, Yuanzhi Li, Shean Wang, Lu Wang, and Weizhu Chen. Lora: Low-rank adaptation of large language models. In *Proceedings of ICLR*, 2022.

Sehoon Kim, Connor R. C. Hooper, Amir Gholami, Zhen Dong, Xiuyu Li, Sheng Shen, and Kurt Keutzer. Squeezelm: Dense-and-sparse quantization. In *Proceedings of the Forty-first International Conference on Machine Learning (ICML)*, 2023.

Yixiao Li, Yifan Yu, Chen Liang, Pengcheng He, Nikos Karampatziakis, Weizhu Chen, and Tuo Zhao. Loftq: Lora-fine-tuning-aware quantization for large language models, 2023. URL <https://arxiv.org/abs/2310.08659>.

Ji Lin, Jie Tang, Haotao Tang, Shuxin Yang, Xiaoxia Dang, and Song Han. Awq: Activation-aware weight quantization for llm compression and acceleration. *arXiv preprint arXiv:2306.00978*, 2023.

Spyros Makridakis, Fotios Petropoulos, and Yanfei Kang. Large language models: Their success and impact. *Forecasting*, 5(3):536–549, 2023.

Todor Mihaylov, Peter Clark, Tushar Khot, and Ashish Sabharwal. Can a suit of armor conduct electricity? a new dataset for open book question answering. In *Proceedings of the 2018 Conference on Empirical Methods in Natural Language Processing*, pages 2381–2391, 2018.

Mohaimenul Azam Khan Raiaan, Md Saddam Hossain Mukta, Kaniz Fatema, Nur Mohammad Fahad, Sadman Sakib, Most Marufatul Jannat Mim, Jubaer Ahmad, Mohammed Eunus Ali, and Sami Azam. A review on large language models: Architectures, applications, taxonomies, open issues and challenges. *IEEE Access*, 2024.

Keisuke Sakaguchi, Ronan Le Bras, Chandra Bhagavatula, and Yejin Choi. Winogrande: An adversarial winograd schema challenge at scale. *Communications of the ACM*, 64(9):99–106, 2021.

Rohan Taori, Ishaan Gulrajani, Tianyi Zhang, Yann Dubois, Xuechen Li, Carlos Guestrin, Percy Liang, and Tatsunori B. Hashimoto. Stanford alpaca: An instruction-following llama model. *Stanford CRFM*, 2023. URL [https://github.com/tatsu-lab/stanford\\_alpaca](https://github.com/tatsu-lab/stanford_alpaca).

Hugo Touvron, Louis Martin, Kevin Stone, Peter Albert, Amjad Almahairi, Yasmine Babaei, Nikolay Bashlykov, Soumya Batra, Prajjwal Bhargava, and et al. Bhosale, Shruti. Llama 2: Open foundation and fine-tuned chat models. *arXiv preprint arXiv:2307.09288*, 2023.

Zhongwei Wan, Xin Wang, Che Liu, Samiul Alam, Yu Zheng, Jiachen Liu, Zhongnan Qu, Shen Yan, Yi Zhu, Quanlu Zhang, et al. Efficient large language models: A survey. *Transactions on Machine Learning Research*, 2023.

Zhewei Yao, Reza Yazdani Aminabadi, Ming Zhang, Xiang Wu, Cong Li, and Yuxiong He. Zeroquant: Efficient and affordable post-training quantization for large-scale transformers. In *Advances in Neural Information Processing Systems*, volume 35, pages 27168–27183, 2022.

Rowan Zellers, Ari Holtzman, Yonatan Bisk, Ali Farhadi, and Yejin Choi. Hellaswag: Can a machine really finish your sentence? In *Proceedings of the 57th Annual Meeting of the Association for Computational Linguistics*, pages 4791–4800, 2019.

Qingru Zhang, Minshuo Chen, Alexander Bukharin, Pengcheng He, Yu Cheng, Weizhu Chen, and Tuo Zhao. Adaptive budget allocation for parameter-efficient fine-tuning. In *International Conference on Learning Representations*. Openreview, 2023a.

Qingru Zhang, Minshuo Chen, Alexander Bukharin, Nikos Karampatziakis, Pengcheng He, Yu Cheng, Weizhu Chen, and Tuo Zhao. Adalora: Adaptive budget allocation for parameter-efficient fine-tuning. *arXiv preprint arXiv:2303.10512*, 2023b.

Changhai Zhou, Shijie Han, Shiyang Zhang, Shichao Weng, Zekai Liu, and Cheng Jin. Rankadaptor: Hierarchical dynamic low-rank adaptation for structural pruned llms. *arXiv preprint arXiv:2406.15734*, 2024.

## 7 Trajectories

To compare the training trajectories of the full-precision model, the standard quantized model, and LoFTQ with varying numbers of iterations, we periodically saved “parameter snapshots” from each model during fine-tuning. Specifically, at every 50 training steps, we extracted all trainable weights—including the LoRA/Adapter A/B matrices for LoFTQ—and saved them to disk, yielding around 10–20 snapshots per model. We then concatenated these snapshots into a  $[3T, D]$  parameter matrix (where  $T$  is the number of snapshots per model and  $D$  is the dimension of the flattened parameter vectors). Next, we applied Principal Component Analysis (PCA) using scikit-learn’s PCA module to learn a 2D projection across all snapshots. For visualization, each model’s snapshots were transformed into the resulting 2D space and plotted in Matplotlib, with the points connected in chronological order to depict the evolution of parameters during training. In the figure, blue circles represent the trajectory of the original full-precision (FP32) model, orange triangles correspond to the fully quantized model, and green squares, red diamonds, and purple crosses indicate LoFTQ after 1, 5, and 10 iterations, respectively. From this 2D PCA projection, we observe that LoFTQ-1 remains relatively close to the FP32 path, suggesting that even a single iteration of LoFTQ helps narrow the performance gap. However, increasing the number of LoFTQ iterations does not continuously improve convergence: LoFTQ-5 and especially LoFTQ-10 deviate more substantially from both FP32 and fully quantized trajectories, with LoFTQ-10 extending abnormally far along the PCA axes. These findings suggest that while LoFTQ offers an initial boost by moving closer to the uncompressed model, additional iterations may lead the optimization path away from more optimal parameter regions, limiting further gains in performance.

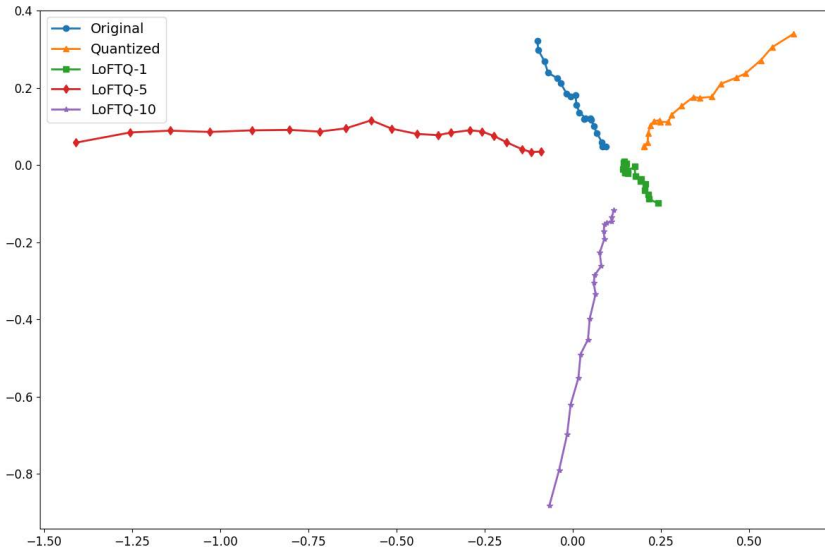


Figure 5: 2D PCA projection of parameter trajectories from three models during fine-tuning. We saved weight snapshots at regular intervals, concatenated them into a  $[3T, D]$  matrix, and used PCA to reduce the dimensionality to two. The blue curve (circles) represents the original full-precision model, the orange curve (triangles) denotes the standard quantized model, and the green squares, red diamonds, and purple crosses correspond to LoFTQ after 1, 5, and 10 iterations, respectively. While LoFTQ-1 stays relatively close to the FP32 path, additional LoFTQ iterations do not sustain that initial convergence advantage, as LoFTQ-5 and LoFTQ-10 deviate more significantly and form longer, more anomalous trajectories in the PCA space.

## 8 quantization

We first apply NF-quantization with bit size  $b_0$  and bucket size  $B_0$  to obtain the quantized matrix  $\widehat{A}_i$  and the absmax values for each block  $s = [s_1, \dots, s_{\frac{\text{sizeof}(A_i)}{B_0}}]$ . These absmax values are further quantized to  $b_1$  bits via uniform integer quantization with bucket size  $B_1$  to obtain the quantized

vector  $\hat{s}$ , along with the absmax values for  $s$ , i.e.,  $v = [v_1, \dots, v_{\frac{\text{sizeof}(A_i)}{B_0 B_1}}]$ . Finally, we cast  $v$  to  $b_2$  bits to obtain  $\hat{v}$ .

This quantization scheme requires storing  $\hat{A}_i, \hat{s}, \hat{v}$  to represent  $A_i$ . We can thus quantify the memory cost (number of bits) for storing  $A_i$  given a configuration  $c_i = (b_0, b_1, b_2, B_0, B_1)$  as:

$$\text{memory\_cost}(A_i, c_i) = \text{sizeof}(A_i) \cdot \left( b_0 + \frac{b_1}{B_0} + \frac{b_2}{B_0 \cdot B_1} \right) \quad (16)$$

The original NF-4 double quantization is a special case with  $q_{\text{NF4}} = (4, 8, \text{fp32}, 64, 256)$  and  $\text{memory\_cost}(A_i, q_{\text{NF4}}) = 4.127 \cdot \text{sizeof}(A_i)$ , i.e., NF-4 requires on average 4.127 bits per parameter.

## 9 Pseudo code of the specific algorithm in the QR-Adaptor framework

Due to page limitations, we present the pseudocode of the algorithm in Section 3 below.

---

### Algorithm 1 Pareto Rank Calculation

---

```

1: Input: Population  $P$  with  $n$  individuals
2: Calculate the number of dominated individuals  $n_p$  and the set of solutions dominated  $S_p$  for each individual  $p$ 
3: Place individuals with  $n_p = 0$  into set  $F_1$ 
4: for each individual  $i$  in  $F_1$  do
5:   for each individual  $j \in S_i$  do
6:      $n_j \leftarrow n_j - 1$ 
7:     if  $n_j = 0$  then
8:       Add individual  $j$  to set  $F_2$ 
9:     end if
10:   end for
11: end for
12: Repeat for  $F_2, F_3, \dots$ , until all individuals are ranked
13: Output: Pareto-ranked individuals

```

---



---

### Algorithm 2 Crowding Distance Calculation

---

```

1: Input: Ranked individuals  $F$  with  $N$  individuals,  $M$  objectives
2: for each individual  $n \in 1 \dots N$  do
3:   Initialize  $d_n \leftarrow 0$ 
4: end for
5: for each objective function  $f_m$  do
6:   Sort individuals based on  $f_m$ 
7:    $f_m^{\max}, f_m^{\min} \leftarrow \max f_m, \min f_m$ 
8:    $d_1, d_N \leftarrow \infty$ 
9:   for  $n = 2$  to  $N - 1$  do
10:     $d_n \leftarrow d_n + \frac{f_m(n+1) - f_m(n-1)}{f_m^{\max} - f_m^{\min}}$ 
11:   end for
12: end for
13: Output: Crowding distances  $d_n$  for each individual  $n$ 

```

---



---

### Algorithm 3 Simulated Binary Crossover (SBX)

---

**Require:** Two parent individuals  $P_1$  and  $P_2$ , each with  $L$  real-valued genes

```

1: Initialize offspring  $O_1$  and  $O_2$  as empty
2: for  $l = 1$  to  $L$  do
3:   Generate a random number  $u \in [0, 1]$ 
4:   if  $u \leq 0.5$  then
5:      $\beta \leftarrow (2u)^{1/(n+1)}$ 
6:   else
7:      $\beta \leftarrow \left( \frac{1}{2(1-u)} \right)^{1/(n+1)}$ 
8:   end if
9:    $y_{1l} \leftarrow 0.5 \cdot ((1 + \beta) \cdot p_{1l} + (1 - \beta) \cdot p_{2l})$ 
10:   $y_{2l} \leftarrow 0.5 \cdot ((1 - \beta) \cdot p_{1l} + (1 + \beta) \cdot p_{2l})$ 
11:  Append  $y_{1l}$  to  $O_1$  and  $y_{2l}$  to  $O_2$ 
12: end for
13: Output:  $O_1$  and  $O_2$ 

```

---



---

### Algorithm 4 Polynomial Mutation

---

**Require:** Individual  $P$  with  $L$  real-valued genes, mutation probability  $p_m$

```

1: Initialize mutated individual  $P'$  as a copy of  $P$ 
2: for  $l = 1$  to  $L$  do
3:   Generate a random number  $u \in [0, 1]$ 
4:   if  $u < p_m$  then
5:     Generate a random number  $\delta \in [-1, 1]$ 
6:      $x'_l \leftarrow x_l + (x_{\max} - x_{\min}) \cdot \delta \cdot (1 - |\delta|)^{n-1}$ 
7:     Replace  $x_l$  with  $x'_l$  in  $P'$ 
8:   end if
9: end for
10: Output: Mutated individual  $P'$ 

```

---

Table 2: Performance comparison of different methods across various bit-width configurations on Llama2-7B. Superscripts on LoftQ bits indicate the number of initialization iterations. QR-Adaptor searches for optimal bit number and rank value for each layer based on different tasks with its bit number averaged across tasks. Bold figures represent the best performance for a given model and task, while underlined figures indicate the second-best. Accuracy is reported as %.

	Method	Bit	ARC(C)	ARC(E)	BoolQ	HellaS	OBQA	PIQA	WinoG	Average
Rank = 8	LoRA	16	46.93	<u>77.36</u>	<u>78.47</u>	<b>76.93</b>	44.80	79.38	69.38	67.61
	QLoRA	8	<b>48.21</b>	<u>77.36</u>	77.92	<u>76.88</u>	44.80	<u>79.82</u>	68.75	<u>67.70</u>
	QLoRA	4	46.25	76.26	77.43	76.42	<b>46.20</b>	78.67	<u>69.85</u>	67.30
	AdaLoRA	16	46.08	76.77	77.46	75.89	44.20	79.16	69.22	66.97
	AdaLoRA	8	46.08	76.73	77.49	75.93	44.20	79.00	69.06	66.93
	AdaLoRA	4	46.33	75.25	76.39	75.45	44.40	77.91	69.14	66.41
	LoftQ	<sup>4<sup>1</sup></sup>	46.16	77.10	77.43	76.68	44.80	79.33	69.30	67.26
	LoftQ	<sup>4<sup>5</sup></sup>	47.35	76.64	76.33	76.36	45.60	79.05	69.06	67.20
	LQ-LoRA	4	47.18	76.60	76.54	76.24	45.00	78.84	68.90	67.04
Rank = 16	QR-Adaptor	5.45	<u>48.04</u>	<b>77.44</b>	<b>78.96</b>	76.84	<u>46.00</u>	<b>79.86</b>	<b>69.97</b>	<b>68.15</b>
	LoRA	16	46.93	<b>77.57</b>	<u>78.41</u>	76.81	45.00	79.38	69.06	67.59
	QLoRA	8	47.61	<u>77.44</u>	<u>78.41</u>	<b>76.93</b>	45.40	79.05	69.06	<u>67.70</u>
	QLoRA	4	46.67	76.35	77.25	76.40	45.00	78.84	<u>70.01</u>	67.22
	AdaLoRA	16	46.16	76.68	77.58	75.92	44.20	79.11	69.38	67.00
	AdaLoRA	8	46.16	76.68	77.40	75.91	44.40	79.11	69.06	66.96
	AdaLoRA	4	46.33	75.29	76.45	75.44	44.20	77.91	69.46	66.47
	LoftQ	<sup>4<sup>1</sup></sup>	47.10	77.19	77.89	76.61	44.80	<u>79.43</u>	69.69	67.53
	LoftQ	<sup>4<sup>5</sup></sup>	<u>47.95</u>	76.47	76.79	76.25	45.60	78.51	69.61	67.31
	LQ-LoRA	4	47.10	76.39	77.22	76.33	<b>46.40</b>	78.78	<b>70.09</b>	67.47
	QR-Adaptor	5.45	<b>48.04</b>	<u>77.44</u>	<b>78.96</b>	76.84	<u>46.00</u>	<b>79.86</b>	69.97	<b>68.15</b>

## 10 More Results

Due to page limitations, we present remaining results across various models here.

### 10.1 Experiment Scope Expansion: Llama 2 Series

In the original experiments, the focus was primarily on Llama3.1, considering that its updated architecture present new challenges for quantization. Compared to Llama2 series, Llama3.1 is significantly harder to quantize, especially under low-bit configurations, as they incorporate more sophisticated architectural features. Additionally, to comprehensively demonstrate the superiority of **QR-Adaptor**, we have also conducted extensive performance experiments on the Llama2 series models, with the results presented in Table 2 and Table 3.

Our results show that **QR-Adaptor** consistently demonstrates superior performance across all tasks and outperforms existing methods, such as AdaLoRA and LoftQ, on Llama 2 series. The robustness of **QR-Adaptor** is also evident, especially on tasks that typically cause performance degradation for other methods.

### 10.2 Visualization Results for the MMLU Task

The results for the MMLU task in LLaMA2 are shown in Figure 6. **QR-Adaptor** demonstrates outstanding performance across various benchmarks. Due to the rank value selection ranging from 2 to 16, in some cases, **QR-Adaptor** consumes less memory than the fine-tuned 4-bit quantized models. Moreover, the low-precision models fine-tuned by **QR-Adaptor** outperform the fine-tuned 16-bit models. Another advantage of the **QR-Adaptor** is that it can be implemented without any additional technical measures to optimize performance, apart from spending some time (about 15 minutes to get one data point). This simple but effective method is very useful in practical applications.

Table 3: Performance comparison of different methods across various bit-width configurations on Llama2-13B. Superscripts on LoftQ bits indicate the number of initialization iterations. QR-Adaptor searches for optimal bit number and rank value for each layer based on different tasks with its bit number averaged across tasks. Bold figures represent the best performance for a given model and task, while underlined figures indicate the second-best. Accuracy is reported as %.

	Method	Bit	ARC(C)	ARC(E)	BoolQ	HellaS	OBQA	PIQA	WinoG	Average
Rank = 8	LoRA	16	<u>52.56</u>	<u>80.18</u>	<u>81.44</u>	<u>79.98</u>	<b>46.40</b>	<u>81.12</u>	71.98	<u>70.52</u>
	QLoRA	8	52.39	<u>80.18</u>	81.22	79.92	45.00	80.47	<b>73.09</b>	70.32
	QLoRA	4	51.54	78.91	81.41	79.46	45.40	80.30	71.82	69.83
	AdaLoRA	16	49.15	79.46	80.37	79.25	45.40	80.47	72.30	69.49
	AdaLoRA	8	49.32	79.34	80.43	79.29	45.60	80.47	72.22	69.52
	AdaLoRA	4	48.29	77.78	80.40	78.12	44.20	80.14	71.74	68.67
	LoftQ	<sup>4<sup>1</sup></sup>	50.68	78.79	81.16	79.12	<u>45.80</u>	80.41	71.35	69.62
	LoftQ	<sup>4<sup>5</sup></sup>	50.34	78.87	80.24	78.81	45.20	80.25	70.80	69.22
	LQ-LoRA	4	50.60	78.79	80.67	78.91	45.00	80.14	71.11	69.32
Rank = 16	QR-Adaptor	6.125	<b>52.82</b>	<b>80.64</b>	<b>81.84</b>	<b>80.08</b>	<u>45.80</u>	<b>81.45</b>	72.69	<b>70.76</b>
	LoRA	16	<u>52.13</u>	79.84	<u>81.50</u>	<u>80.07</u>	<b>46.20</b>	<u>81.23</u>	71.98	<u>70.42</u>
	QLoRA	8	51.54	<u>80.01</u>	81.13	79.86	<b>46.20</b>	81.18	72.22	70.31
	QLoRA	4	51.45	79.04	81.04	79.48	45.60	80.47	71.82	69.84
	AdaLoRA	16	49.40	79.34	80.46	79.28	45.40	80.47	72.30	69.52
	AdaLoRA	8	49.49	79.29	80.40	79.27	45.40	80.52	<u>72.38</u>	69.54
	AdaLoRA	4	48.29	77.69	80.43	78.10	44.20	80.09	71.67	68.64
	LoftQ	<sup>4<sup>1</sup></sup>	50.68	78.87	80.86	79.18	<u>45.80</u>	80.30	71.90	69.66
	LoftQ	<sup>4<sup>5</sup></sup>	50.60	78.96	80.92	79.15	45.40	80.41	71.59	69.58
	LQ-LoRA	4	50.09	78.79	80.43	79.06	45.40	80.14	71.67	69.37
	QR-Adaptor	6.125	<b>52.82</b>	<b>80.64</b>	<b>81.84</b>	<b>80.08</b>	<u>45.80</u>	<b>81.45</b>	72.69	<b>70.76</b>

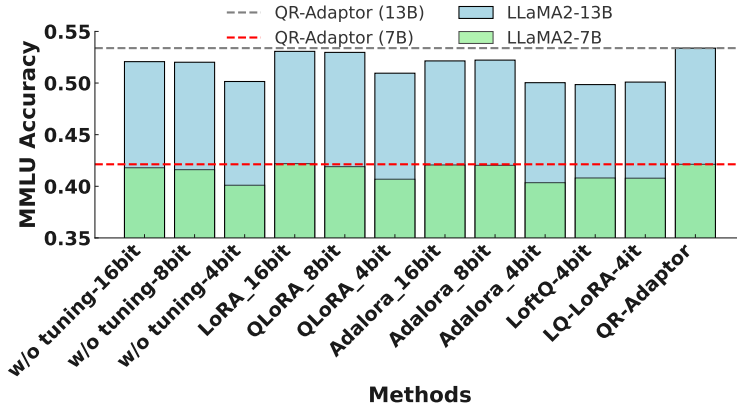


Figure 6: Performance comparison on MMLU benchmark. QR-Adaptor outperforms other methods.

### 10.3 Effectiveness on Larger Datasets with Higher Ranks

To address the concern regarding the effectiveness of small LoRA ranks on larger datasets, we conducted additional experiments on the LLaMA3.1-8B model using a larger dataset consisting of 177k samples. We tested our method with higher LoRA ranks (32 and 64) to evaluate its performance in handling large-scale data.

Our results are summarized in Table 4. The table compares the performance of **QR-Adaptor** with other baseline methods, including LoRA, QLoRA, AdaLoRA, and LoftQ, across various tasks. The performance metrics include accuracy scores on datasets such as ARC (Challenge), ARC (Easy), BoolQ, HellaSwag, OpenBookQA, PIQA, WinoGrande, and MMLU.

Table 4: Performance comparison of different methods across various bit-width configurations on Llama3.1-8B with higher ranks. Superscripts on LoftQ bits indicate the number of initialization iterations. QR-Adaptor searches for optimal bit number and rank value for each layer based on different tasks with its bit number averaged across tasks. Bold figures represent the best performance for a given model and task, while underlined figures indicate the second-best. Accuracy is reported as %.

Method	Rank	Bit	ARC(C)	ARC(E)	BoolQ	HellaS	OBQA	PIQA	WinoG	MMLU	Average
LoRA	32	16	54.86	82.74	82.75	<u>79.21</u>	44.40	<u>81.99</u>	74.11	63.66	70.47
LoRA	64	16	<u>55.46</u>	82.95	<u>82.94</u>	79.13	45.00	81.88	<u>74.51</u>	<u>64.34</u>	<u>70.78</u>
QLoRA	32	8	55.20	<u>83.12</u>	81.93	79.07	<b>46.20</b>	81.88	73.32	63.28	70.50
QLoRA	32	4	53.41	80.89	82.05	78.42	43.60	80.90	73.01	60.97	69.16
QLoRA	64	8	<u>55.46</u>	83.04	81.96	79.17	<u>45.80</u>	81.94	73.01	63.34	70.47
QLoRA	64	4	53.41	81.19	81.74	78.35	44.60	80.69	72.06	60.79	69.10
AdaLoRA	32	8	53.92	81.82	82.20	78.57	<b>46.20</b>	81.50	73.40	63.82	70.18
AdaLoRA	32	4	51.45	81.02	80.86	77.30	42.40	80.96	72.53	58.15	68.08
AdaLoRA	64	8	53.92	82.11	81.93	78.74	46.20	81.39	73.95	63.88	70.27
AdaLoRA	64	4	52.13	80.98	81.04	77.20	42.20	80.85	72.77	58.07	68.16
LoftQ	32	<sup>4</sup> <sup>1</sup>	53.84	81.36	81.41	78.12	43.00	81.50	73.56	59.40	69.02
LoftQ	32	<sup>4</sup> <sup>5</sup>	52.56	81.36	81.96	78.05	42.80	81.45	73.09	59.41	68.84
LoftQ	32	<sup>4</sup> <sup>10</sup>	51.62	81.31	82.51	78.16	43.60	81.34	72.30	59.12	68.75
LoftQ	64	<sup>4</sup> <sup>1</sup>	52.82	81.40	81.59	78.23	43.20	81.34	73.88	59.78	69.03
LoftQ	64	<sup>4</sup> <sup>5</sup>	52.39	81.10	81.13	78.33	43.40	81.34	73.24	58.69	68.70
LoftQ	64	<sup>4</sup> <sup>10</sup>	51.71	81.23	81.62	78.37	43.20	81.01	72.77	59.25	68.65
QR-Adaptor	32	5.875	<b>56.12</b>	<u>83.45</u>	<u>83.21</u>	<u>79.78</u>	<b>46.20</b>	<b>82.10</b>	<u>74.59</u>	<b>64.40</b>	<b>71.23</b>

## Key Observations

- **Effectiveness of LoRA Initialization:** Despite using higher ranks (32 and 64) and larger datasets, methods like LoftQ and LQ-LoRA do not consistently outperform the standard QLoRA baseline or the quantized models without fine-tuning. Increasing iterations in LoftQ (from LoftQ-1 to LoftQ-10) to better fit quantization errors leads to performance degradation, especially on challenging tasks like MMLU and GSM8K. These results suggest that fitting quantization errors using LoRA initialization is not universally effective and may introduce noise that hinders model performance.
- **Effectiveness on Larger Datasets:** Our method, **QR-Adaptor**, consistently achieves superior performance across all tasks and outperforms other methods, confirming its robustness and scalability. The results validate that **QR-Adaptor** is effective even when small LoRA ranks might not suffice for larger datasets.
- **Impact of Adaptive LoRA Rank Reduction:** AdaLoRA exhibits performance drops, particularly with lower bit-widths and on more challenging tasks. This supports our observation that dynamically adjusting the rank during fine-tuning can lead to convergence issues in quantized models, which are less robust due to quantization errors.

These results reinforce our initial observations and highlight the limitations of methods that attempt to fit quantization errors through LoRA initialization. The inability of LoftQ and AdaLoRA to improve performance significantly, even with higher ranks and larger datasets, underscores the challenges associated with such approaches. In contrast, **QR-Adaptor**, guided by our proposed constraints, demonstrates consistent performance improvements.

## 10.4 Training Time Comparison

An important consideration in the evaluation of QR-Adaptor is the training time, particularly due to its reliance on Bayesian optimization. While QR-Adaptor provides significant performance improvements, it may require additional time per iteration compared to other methods. Table 5 summarizes the training time per iteration for QR-Adaptor and baseline methods on Llama2-7B.

Although QR-Adaptor takes longer to train due to its optimization process, this trade-off results in superior performance, particularly in terms of task-specific optimizations. The Bayesian optimization employed by QR-Adaptor ensures more precise adjustments to the model, which leads to better results on downstream tasks without additional resource consumption during the optimization process.

Table 5: Training time per iteration for different methods on Llama2-7B.

Method	Time per Iteration (min)
LoftQ	9
QR-Adaptor	15

### 10.5 Fairer Comparison: Matching Bit-width Configurations

Another important consideration for a fair comparison of quantization methods is the bit-width configuration used. To ensure that prior methods are evaluated under the same conditions as QR-Adaptor, we have re-evaluated AdaLoRA and LoftQ using the same mixed-precision configurations that were optimized through QR-Adaptor’s framework. The updated results for Llama 2-13B are shown in Table 6.

Table 6: Performance comparison with fair bit-width configurations for Llama2-13B. Accuracy is reported as %

Method	BoolQ	PIQA	HellaS	WinoG	ARC(E)	ARC(C)	OBQA	Average
AdaLoRA	81.08	80.13	79.21	71.74	79.51	50.12	45.60	69.77
LoftQ	80.93	79.47	79.02	71.34	79.26	51.20	45.60	69.98
QR-Adaptor	<b>81.84</b>	<b>81.45</b>	<b>80.08</b>	<b>72.69</b>	<b>80.64</b>	<b>52.82</b>	<b>45.80</b>	<b>70.76</b>

The results indicate that the initialization constraints applied by QR-Adaptor provide substantial improvements over the original configurations of AdaLoRA and LoftQ. Despite these improvements, QR-Adaptor still outperforms these methods in terms of overall task performance. The constraints, specifically ensuring stable initialization and fixing trainable parameters, contribute significantly to the enhanced performance of QR-Adaptor.

### 10.6 Impact of Longer Fine-tuning Epochs on Unfixed Parameters

While increasing the fine-tuning epochs for AdaLoRA can lead to some performance improvements, these gains are marginal and AdaLoRA still does not outperform other methods like LoRA, QLoRA, or our proposed QR-Adaptor.

#### Findings

- **Marginal Improvement with Increased Epochs:** Extending the training of AdaLoRA from 2 epochs to 5 epochs results in a slight performance increase. However, this improvement is not substantial and comes at the cost of significantly longer training times.
- **Need for Mixed-Precision with Adaptive Rank:** The results suggest that adaptive rank adjustment alone, as in AdaLoRA, may not be the most effective approach. The combination of adaptive rank with mixed-precision quantization, as in QR-Adaptor, yields superior performance.

#### Supporting Data

We provide an updated table below that includes an "Epochs" column, showing the results for LoRA, QLoRA, AdaLoRA (at 2 and 5 epochs), and QR-Adaptor.

#### Observation

- **AdaLoRA’s Performance with Increased Epochs:** As observed, AdaLoRA shows only slight performance improvements when training is extended from 2 to 5 epochs. Even with

Table 7: Performance comparison of different methods with varying fine-tuning epochs on Llama3.1-8B. Accuracy is reported as %

Method	Rank	Bit-width	Epochs	ARC (C)	ARC (E)	BoolQ	GSM8K (S)	GSM8K (F)	HellaS	OBQA	PIQA	WinoG
LoRA	8	16	2	56.14	83.88	83.18	54.36	54.28	79.44	45.20	82.10	<b>75.30</b>
QLoRA	8	8	2	57.08	83.46	82.48	53.75	53.90	79.63	<b>46.00</b>	82.10	74.59
QLoRA	8	4	2	54.35	82.41	82.08	44.35	44.50	78.82	44.20	81.50	73.64
AdaLoRA	8	16	2	52.90	81.99	81.87	50.57	50.57	78.65	45.00	81.34	73.95
AdaLoRA	8	16	5	53.50	82.25	82.05	51.00	50.90	78.75	45.20	81.40	74.10
AdaLoRA	8	8	2	52.90	81.86	82.05	49.96	49.96	78.65	44.80	81.34	74.43
AdaLoRA	8	8	5	53.10	82.00	82.10	50.20	50.10	78.70	45.20	81.38	74.50
AdaLoRA	8	4	2	51.28	80.98	80.61	37.83	38.36	77.36	42.80	80.74	72.53
AdaLoRA	8	4	5	51.50	81.10	80.75	38.00	38.50	77.40	43.20	80.78	72.60
QR-Adaptor	8	5.375	2	<b>56.83</b>	<b>84.12</b>	<b>83.38</b>	<b>56.29</b>	<b>56.11</b>	<b>80.93</b>	<b>45.80</b>	<b>82.92</b>	75.10

the increase in epochs, AdaLoRA’s performance does not surpass that of LoRA, QLoRA, or QR-Adaptor at 2 epochs.

- **QR-Adaptor’s Consistency:** QR-Adaptor consistently achieves superior performance across all tasks, further validating the effectiveness of our method over other adaptive rank-based approaches.
- **16-bit AdaLoRA Performance:** Notably, AdaLoRA with 16-bit precision (not quantized) still underperforms compared to LoRA and QLoRA, suggesting that the adaptive rank mechanism alone is not enough, and the integration of mixed-precision quantization is crucial.

## 10.7 Impact of 2-Bit Quantization and LoftQ Iterations

We have conducted additional experiments to explore the performance of LoftQ with 2-bit quantization and its variations across different numbers of iterations.

In these experiments, we used the NF2 variant from LoftQ, based on QLoRA’s NF4, to implement 2-bit quantization, since QLoRA does not natively support this low-bit quantization (as stated in the original paper and the GitHub repository). The 2-bit results in the LoftQ paper were also based on this NF2 variant. We fine-tuned the models using a 52k dataset, with the rank for LoftQ set to 16. The superscripts on LoftQ’s bit-width values represent the number of LoftQ iterations, with 0 iterations considered approximately equivalent to QLoRA (since QLoRA does not provide a 2-bit quantization type).

The results of our experiments are summarized in Table 8.

Table 8: Performance comparison for 2-bit quantization and LoftQ iterations on LLaMA3.1-8B with 52k fine-tuning dataset. Superscripts on LoftQ bits indicate the number of initialization iterations. Accuracy is reported as %

Method	Bit-width	MMLU	GSM8K	ARC(C)	ARC(E)	BoolQ	HellaS	OBQA	PIQA	WinoG
LoftQ	$2^0$	23.76	0.00	26.24	25.25	37.83	26.86	29.40	52.55	49.18
LoftQ	$2^1$	24.71	0.00	25.17	25.25	37.83	25.73	29.20	51.58	49.33
LoftQ	$2^5$	24.65	0.00	25.17	24.83	37.83	26.30	28.20	51.41	49.41
LoftQ	$2^{10}$	<u>24.80</u>	0.00	<b>26.02</b>	25.25	37.83	26.53	<b>29.80</b>	<b>52.83</b>	48.86
QR-Adaptor	3.625	<b>62.58</b>	0.53	<b>55.93</b>	<b>82.43</b>	<b>82.13</b>	<b>79.23</b>	<b>45.60</b>	<b>81.83</b>	<b>74.79</b>

## Key Observations

- **MMLU Performance:** For the MMLU dataset, which involves multiple-choice questions, models with 2-bit quantization perform at approximately 25% accuracy, which is close to random guessing. Thus, LoftQ’s 2-bit quantization yields little practical improvement for MMLU on LLaMA3.1. This suggests that the performance of LoftQ with 2-bit quantization is not robust on complex tasks.

- **GSM8K Performance:** On the GSM8K dataset, LoftQ’s 2-bit quantization fails to provide any meaningful performance, resulting in 0% accuracy. This highlights the challenges of quantizing LLaMA3.1 to such low precision, especially on complex question-answering tasks.
- **Common Sense Reasoning Tasks:** For simpler reasoning tasks like WinoGrande, the LoftQ 2-bit quantized models show some capacity to answer, but there is no significant difference across LoftQ’s iterations, and the models still perform similarly to random guessing on most datasets.
- **QR-Adaptor Optimization:** For QR-Adaptor, we optimized based on theoretical memory savings from 4-bit quantization. Since 2-bit quantization does not reduce memory usage effectively, we used the theoretical savings in our optimization process. This optimization allowed QR-Adaptor to achieve better performance even when compared to LoftQ with 2-bit quantization.

## Conclusion

From these results, we observe that LoftQ’s 2-bit quantization shows poor performance across the board. Even with multiple iterations (up to 10), LoftQ struggles to achieve reasonable accuracy on tasks like MMLU and GSM8K. In contrast, QR-Adaptor, with its unified optimization of both rank and bit-width during fine-tuning, consistently outperforms LoftQ and other methods.

Notably, while LoftQ’s 2-bit quantization performs poorly, QR-Adaptor manages to retain much better performance by leveraging the advantages of mixed-precision quantization, making it a more effective solution for LLaMA3.1. These findings suggest that for models requiring high precision, such as LLaMA3.1, extreme quantization to 2-bit precision may not be viable, and more moderate bit-widths, as used by QR-Adaptor, provide better results.

We hope these results contribute to the ongoing discussions in the community regarding effective quantization strategies and provide further insights into the practical use of quantized models.

## 11 Version of LLMs

We provide the Hugging Face link of LLMs used in the experiment: LLaMA2-7B: <https://huggingface.co/NousResearch/Llama-2-7b-hf>; LLaMA2-13B: <https://huggingface.co/NousResearch/Llama-2-13b-hf>; LLaMA3.1-8B: <https://huggingface.co/meta-llama/Llama-3.1-8B>.

## 12 More Implementation Details

In optimizing the pruned Llama2-7B model, a carefully designed hyperparameter configuration has been implemented to strike a balance between model performance and computational efficiency. The model is fine-tuned using a learning rate of  $3 \times 10^{-4}$ , with a batch size of 128, divided into micro-batches of 4 to effectively manage memory limitations. Input sequences are capped at 256 tokens, and a dropout rate of 0.05 is applied to the LoRA layers, specifically targeting the query, key, value, and output projections, as well as the gate, down, and up projections. Layer-specific quantization is applied at both 4-bit and 8-bit levels, optimizing memory usage while maintaining computational accuracy. The training is performed using the paged AdamW optimizer with 32-bit precision, ensuring both stability and efficiency. These settings have been rigorously tested and refined through the Optuna framework to achieve an optimal balance between model performance and resource efficiency.

## 13 More Ablation

We conducted comprehensive ablation studies to evaluate the impact of initialization metrics and the sensitivity of the proposed Pareto Ranking Genetic Algorithm (PRGA) to key hyperparameters, including iteration counts and population size. These experiments aim to further substantiate the effectiveness of our proposed approach.

### 13.1 Gradient Norms vs. Relative Entropy

To assess the efficacy of initialization metrics, we compared the use of gradient norms and relative entropy in quantifying layer importance for fine-tuning quantized LLMs. The experimental results are summarized in Table 9.

Table 9: Comparison of gradient norms and relative entropy as initialization metrics on Llama2-13B. Bold values indicate the best performance for each task. Accuracy is reported as %

Initialization Metric	BoolQ	PIQA	HellaS	WinoG	ARC(E)	ARC(C)	OBQA	Average
Gradient Norms	80.79	80.13	79.16	71.69	78.72	50.97	45.40	69.51
Relative Entropy	<b>81.08</b>	<b>80.83</b>	<b>79.80</b>	<b>71.98</b>	<b>79.13</b>	<b>51.65</b>	<b>45.60</b>	<b>70.07</b>

#### Insights:

- **Limitations of Gradient Norms:** Gradient norms exhibit limited variability and are prone to biases induced by quantization, which undermines their reliability as an initialization metric for quantized models.
- **Advantages of Relative Entropy:** Relative entropy captures task-specific layer importance more effectively, resulting in robust initialization and improved performance in downstream optimization.

### 13.2 Sensitivity to Iteration Counts and Population Size

To analyze the sensitivity of PRGA to hyperparameters, we systematically varied the number of iterations and population sizes. Table 10 presents the results of these experiments.

Table 10: Sensitivity analysis of PRGA under different iteration counts and population sizes on Llama3.1-8B. Bold values indicate the best configuration.

Iterations	Population Size	Average Improvement (%)	Total Time (min)
5	3	+0.8	120
5	5	+1.2	150
10	5	+1.5	225
5	20	+1.6	375
10	20	<b>+2.3</b>	450

#### Insights:

- **Trade-offs in Population Size:** Smaller population sizes (e.g., 3) reduce computational cost but may fail to adequately explore the search space. Larger population sizes (e.g., 20) improve exploration and convergence but increase computational overhead.
- **Impact of Iteration Count:** Increasing the number of iterations improves optimization quality, as reflected in better Pareto fronts. However, the marginal benefits diminish beyond 10 iterations, indicating limited practical gains for further increases.
- **Balanced Configuration:** A population size of 5 and 5 iterations strikes a balance between performance improvement and computational efficiency. This configuration can be adjusted based on specific resource availability or performance requirements.

## 14 Reproducibility Statement

To ensure the reproducibility of our results, we provide comprehensive documentation on the steps required to replicate our experiments. Our code is available in scripts such as `optuna_main-v3.py`, `post_training_mixed_quant.py`, and `run_optuna.py`, which handle hyperparameter optimization, mixed-precision quantization, and evaluation. For data preparation, we utilize the Alpaca Cleaned Dataset from `yahma/alpaca-cleaned`, which is automatically downloaded and processed using the `datasets` library. Our environment setup requires an NVIDIA GPU with

CUDA support, preferably with at least 20 GB of memory for the Llama2 model, as well as Python 3.8+ and dependencies like PyTorch, Transformers, Optuna, BitsAndBytes, PEFT, and other libraries, which can be installed via the `requirements.txt` file. The model we fine-tune is the Llama2 architecture (`NousResearch/Llama-2-7b-hf`), using a mixed-precision quantization approach via `bitsandbytes` and Low-Rank Adaptation (LoRA) with the `peft` library. The training is conducted using a mixed-precision setup where the model’s `dtype` is set to `torch.bfloat16` to optimize memory usage and computation efficiency. Our hyperparameter optimization framework leverages Optuna to maximize model accuracy while minimizing memory usage, tuning parameters like quantization bits (4 or 8 bits) and LoRA ranks (2 to 16). To replicate our training process, researchers can execute the provided scripts using the specified command-line arguments, which configure the model, output directories, number of trials, and evaluation tasks. Model checkpoints and Optuna results are saved at regular intervals. The training is conducted using the Hugging Face `Trainer`, configured with parameters including a batch size of 4, gradient accumulation steps of 16, warmup steps of 100, and a learning rate of 1e-4, with evaluation and model saving steps set to every 200 steps. Evaluation is conducted using the `lm_eval` library, where metrics such as accuracy are recorded and saved in JSON format. All hyperparameter settings and model configurations are logged in the output directory, along with training progress and memory usage. Random seeds are set to ensure deterministic behavior. By following these steps, including hardware and software specifications, and running the scripts with the provided configurations, researchers can reproduce our experiments and validate the findings related to mixed-precision quantization and parameter-efficient fine-tuning.

## 15 Ethics Statement

This work builds upon pre-trained large language models Llama2 and utilizes publicly available datasets for instruction fine-tuning Alpaca-clean. We do not introduce any new datasets or data collection processes, and therefore do not involve human annotation in this research. Additionally, our study focuses on improving model efficiency through pruning and quantization techniques, without engaging with sensitive content or user-specific data. As such, this paper does not present any ethical concerns beyond those already associated with the broader body of research on large language models and their datasets. All datasets and models used comply with their respective licenses and terms of use.

## 16 Limitation

A constraint of our framework is the relatively long search time required to determine optimal task-specific configurations. This extended duration is necessary to ensure the best fine-tuning setup for each task. We recognize this as a current limitation and are actively working on improving the efficiency of our search algorithm.